Modulation of the extent of structural heterogeneity in α-synuclein fibrils by the small molecule thioflavin T

Received for publication, May 9, 2017, and in revised form, July 15, 2017 Published, Papers in Press, July 31, 2017, DOI 10.1074/jbc.M117.795617

Harish Kumar[‡], Jogender Singh[‡§], Pratibha Kumari[‡¶], and Jayant B. Udgaonkar[‡1]

From the [‡]National Centre for Biological Sciences, Tata Institute of Fundamental Research, Bengaluru 560065, India, the [§]Department of Molecular Genetics and Microbiology, Duke University Medical Center, Durham, North Carolina 27710, and the [¶]Laboratory of Physical Chemistry, Hönggerberg Campus, ETH Zurich, 8093 Zurich, Switzerland

Edited by Paul E. Fraser

The transition of intrinsically disordered, monomeric α-synuclein into β-sheet–rich oligomers and fibrils is associated with multiple neurodegenerative diseases. Fibrillar aggregates possessing distinct structures that differ in toxicity have been observed in different pathological phenotypes. Understanding the mechanism of the formation of various fibril polymorphs with differing cytotoxic effects is essential for determining how the aggregation reaction could be modulated to favor nontoxic fibrils over toxic fibrils. In this study, two morphologically different α-synuclein fibrils, one helical and the other ribbon-like, are shown to form together. Surprisingly, a widely used small molecule for probing aggregation reactions, thioflavin T (ThT), was found to tune the structural heterogeneity found in the fibrils. The ribbon-like fibrils formed in the presence of ThT were found to have a longer structural core than the helical fibrils formed in the absence of ThT. The ribbon-like fibrils are also more toxic to cells. By facilitating the formation of ribbon-like fibrils over helical fibrils, ThT reduced the extent of fibril polymorphism. This study highlights the role of a small molecule such as ThT in selectively favoring the formation of a specific type of fibril by binding to aggregates formed early on one of multiple pathways, thereby altering the structural core and external morphology of the fibrils formed.

The conversion of soluble, functionally active proteins into insoluble, β-sheet–rich, aggregated structures is associated with a variety of neurodegenerative diseases such as Parkinson's disease (PD)[2] and Alzheimer's disease (AD) (1–4). Detailed structural analyses of the characteristics of cross-β-sheet architecture (5–7) present in these aggregates reveal their polymorphism (8). It is now known that fibrils formed by a single protein can show multiple distinct conformations under different growth conditions (9–11) as well as under identical growth conditions (12–15). The importance of studying fibrillar heterogeneity originated from the prion strain phenomenon, in which a single prion protein is known to cause multiple different pathologies by adopting amyloid-like conformations that differ mainly in their external morphologies and molecular structures (16–18). A prion strain propagates a specific pathology faithfully by presenting a specific amyloid template for existing monomer to add on to. Proteins other than the prion protein can also acquire different fibrillar morphologies, showing different levels of toxicity, and propagate faithfully (5, 10). Importantly, fibrils of different morphologies, which differ in their cytotoxicity levels, have been shown to exist in the brains of different AD patients (8, 19). The differences in the toxicity potentials suggest that various fibrils may have different levels of stability, packing, and hydrophobicity (20–22). It is now clear that fibril polymorphism is responsible for different pathological phenotypes (23). It is therefore important to understand the origin of fibril polymorphism.

In PD, the central molecular species is the protein α-synuclein, which is an intrinsically disordered protein of 140 residues. It is expressed mainly in the neurons of the central nervous system (CNS). It acquires helical and β-hairpin structure upon binding to membranes and β-wrap proteins, respectively (27, 28). The function of this protein has not yet been ascertained conclusively, although some studies suggest that it is involved in the process of vesicle release and trafficking (29). α-Synuclein is known to aggregate and form Lewy bodies in dopaminergic neurons of the brain. Lewy bodies are made of cross-β-sheet–rich structured aggregates called amyloid fibrils. The process of α-synuclein fibrillation is associated with a variety of neurodegenerative diseases besides PD, including dementia with Lewy bodies (1), AD, and multiple system atrophy (2, 3). α-Synuclein has been shown to form differently structured amyloid aggregates (10, 12, 13, 15), but there is little understanding of how this happens.

Structural heterogeneity in α-synuclein fibrils originates mainly during the multi-step process of fibrillation in which monomers self-assemble into various on- and off-pathway oligomers that vary in size, shape, structure, stability, and packing (30, 31). Structurally distinct oligomers appear to grow into different types of fibrillar aggregates with structural cores that resemble the oligomers (31). The structural core of α-synuclein fibrils have been characterized by solid-state NMR (10, 12, 32–34), hydrogen–deuterium exchange mass spectrometry (HDX-MS) (31, 35), HDX-NMR (13, 33), electron paramag-

This work was funded by the Tata Institute of Fundamental Research and the Department of Biotechnology, Ministry of Science and Technology, Government of India. The authors declare that they have no conflicts of interest with the contents of this article.

This article contains supplemental Methods, Figs. S1–S9, and Table S1.

[1] Recipient of a J. C. Bose National Fellowship from the Government of India. To whom correspondence should be addressed. Tel.: 91-80-23666150; Fax: 91-80-23636662; E-mail: jayant@ncbs.res.in.

[2] The abbreviations used are: PD, Parkinson's disease; AD, Alzheimer's disease; Aβ, amyloid beta; HDX, hydrogen–deuterium exchange; AFM, atomic force microscopy; ThT, thioflavin T.

netic resonance (EPR) spectroscopy (36, 37), and proteinase K treatment (38). Most of the studies indicate that residues 31–109 form the structural core of fibrils (10, 12, 13, 15, 31–38). However, fibrils with a very different structural core, comprising residues 1–43 and 58–97, have also been characterized (10).

A recent structural model for α-synuclein fibrils based on solid-state NMR, electron microscopy, and X-ray fiber diffraction data suggests a Greek-key topology (32). The atomic structures of fibrils made from peptides corresponding to the NACore and preNAC segments (residues 68–78 and 47–56, respectively) of the protein have been characterized in a microelectron diffraction study (39). Both of these sequence segments are present in the structural core of fibrils formed by full-length α-synuclein (39). α-Synuclein monomers were found to form antiparallel β-sheet structures that stack on top of each other to form a protofilament (39). The protofilaments twist together to form fibrils (39). Cryo-electron microscopy and scanning transmission electron microscopy studies have also been used to characterize the structure of α-synuclein protofibrils. Two protofilaments, each made of three β-strands from the same subunit, form the protofibrils in which sequence segment 8–94 forms the structural core (15). Two protofibrils were found to associate with each other asymmetrically to form fibrils (15). It was hypothesized that the number of protofibrils and their nature of association in the fibrils may determine the final morphology of α-synuclein fibrils and, hence, their structural heterogeneity (15).

The process of α-synuclein fibrillation has been described by the nucleation-dependent polymerization model, which involves a lag phase followed by an exponential phase (40). During the lag phase, monomers undergo structural rearrangements to form transient nuclei, which further grow by the addition of monomers to form fibrils. The molecular structure of the nucleus is likely to determine the molecular structure of the fibrils (41), and modulation of the nucleation and elongation rates by varying the growth conditions is expected to modulate the amount of various fibrillar polymorphs (42).

Under different solution conditions, α-synuclein has been shown to form two types of fibrils, which differ in their morphology, structural core, toxicity, and infectivity (10). Even under the same aggregation conditions, α-synuclein can form morphologically and structurally different fibrils (12, 13, 15). Understanding the molecular mechanism by which different types of aggregates arise and how fibril formation can be modulated is crucial for the development of therapeutics for PD and other protein aggregation diseases.

Small molecules have been used extensively to modulate and inhibit the process of aggregation for several disease-linked proteins (43–45) including α-synuclein (46, 47). The binding of small molecules to fibrils can reduce the amount of toxic oligomers by blocking fibril dissociation (48), by modifying the fibril surface, which acts as an efficient catalyst to generate toxic oligomers (49), or by driving the equilibrium toward fibril formation (45). The small molecule thioflavin T (ThT) is used widely to monitor the aggregation process for many proteins because of its ability to bind to cross-β-sheet structures found in amyloid fibrils, which modulates the fluorescence properties

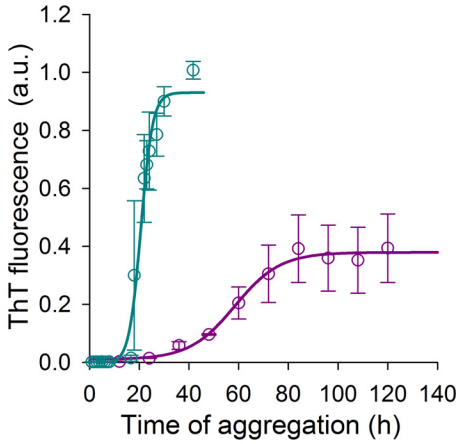

Figure 1. ThT accelerates the fibrillation of α-synuclein. This graph shows ThT fluorescence-monitored kinetics of fibril formation by 100 μM α-synuclein in the absence (*purple*) and presence (*cyan*) of 1 mM ThT at pH 7.0, 37 °C. The *error bars* represent S.D. from three independent aggregation reactions.

of ThT (50). ThT binds to different types of fibrils with different affinities (51), and it can accelerate protein aggregation by binding to monomer or fibrils (52, 53). It is, however, not known whether small molecules such as ThT that bind fibrils can modulate a fibril formation reaction, such that one type of fibrils is preferred over another, or whether the presence of such small molecules during fibril formation affect the internal structure as well as the external morphology of the fibrils.

In this study, the process of α-synuclein fibrillation in the absence and presence of ThT was studied. In the absence of ThT, two types of coexisting fibrils were observed. 70% of the fibrils were helical in external morphology and had a shorter structural core, whereas the remaining 30% of the fibrils had a flat, ribbon-like morphology and an extended structural core. The addition of ThT during aggregation enhances the rate constant of α-synuclein fibril formation and reduces structural heterogeneity with only ribbon-like fibrils being formed.

Results

Effects of ThT on the fibrillation of α-synuclein

To study the effects of ThT on the fibrillation of α-synuclein, 100 μM protein was incubated at pH 7.0 and 37 °C in the absence and presence of 1 mM ThT. The fibrillation process was monitored by measuring the ThT fluorescence emission at 482 nm (Fig. 1). In the absence of ThT, fibril formation by α-synuclein followed a nucleation-dependent polymerization mechanism with a lag phase of ~30 h duration. In contrast, the presence of ThT accelerated the fibrillation of the protein by reducing the lag phase and accelerating the elongation phase. The ThT fluorescence emission signal obtained at saturation for the reaction in the presence of ThT was 2-fold higher than for the reaction in the absence of ThT, indicating that either the amount of fibrils was greater or the fibrils differed in their binding ability to ThT. For fibrils formed in the absence and presence of 1 mM ThT, similar amounts of monomer were found to have converted into fibrils at saturation (supplemental Fig. S1). Hence, it was likely that the fibrils formed in the absence and presence of 1 mM ThT differed in their ability to bind ThT.

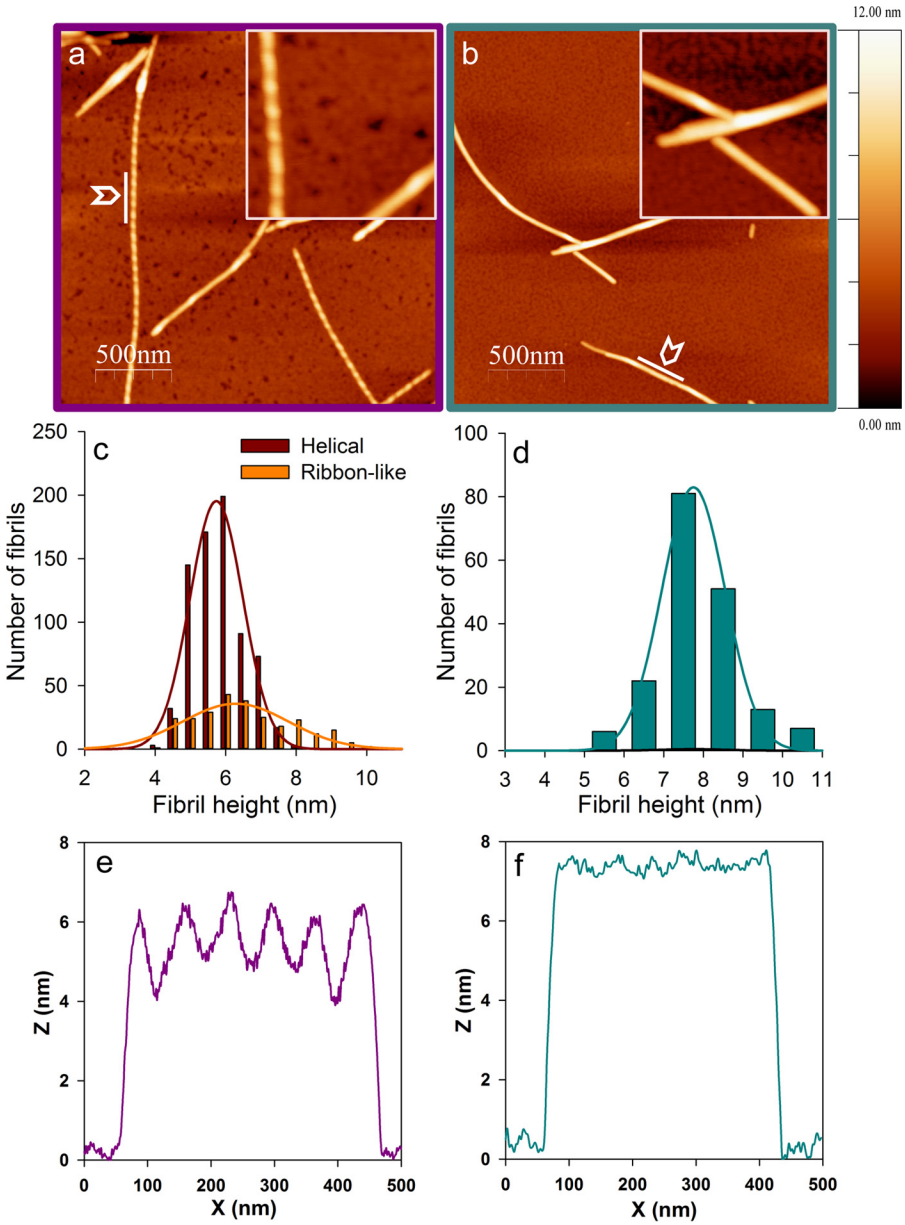

Figure 2. Two different morphologies of α-synuclein fibrils are observed in the absence of ThT. *a* and *b*, AFM images of fibrils formed in the absence of ThT (*a*) and in the presence of 1 mM ThT (*b*) at a time corresponding to three times the t_{50} of ThT fluorescence-monitored kinetics. *c* and *d*, show is the fibril height distribution from *a* and *b*, respectively. *e*, the height profile of a single helical fibril from *a*, where an *arrow* points to the area from which the height profile was taken. *f*, the height profile of a single, flat, ribbon-like fibril from *b*, where an *arrow* points to the area from which the height profile was taken.

Effect of ThT on the size and morphology of the fibrils

Atomic force microscopy (AFM) images were obtained for fibrils formed by 100 μM protein both in the absence and presence of ThT (Fig. 2, *a* and *b*). Two types of fibrils were observed to have formed in the absence of ThT (Fig. 2*c*). One type was helical, with a periodicity of 74 ± 6 nm (Fig. 2*e*), and the other was flat and ribbon-like with no periodicity. The mean heights of the helical and ribbon-like fibrils were 5.7 ± 0.7 and 6.3 ± 1.5 nm, respectively. Interestingly, only one type of fibril was obtained in the presence of ThT; these were flat and ribbon-like with a mean height of 7.4 ± 0.8 nm (Fig. 2, *d* and *f*). Comparable results were obtained when the fibrils were formed from 50 μM protein (data not shown). The flat, ribbon-like fibrils formed in the presence of ThT had a larger diameter and less heterogeneity than the flat, ribbon-like fibrils formed in the absence of ThT (Fig. 2, *c* and *d*); the standard deviation of the fibril height distribution was 0.8 nm in the former case and 1.5 nm in the latter case. The difference in the heights of the ribbon-like fibrils formed in the absence and presence of ThT could conceivably result from intercalation of the ThT molecules in the fibrils formed in the presence of ThT.

To check whether the two types of fibrils behaved like prion strains, seeds were formed by sonicating the fibrils formed in the absence and presence of ThT, and seeding assays were carried out both in the absence and presence of ThT. It was found that both types of seeds (at 3% concentration) abolished the lag phase regardless of whether ThT was present during the aggregation of 100 μM α-synuclein (supplemental Fig. S2). Further-

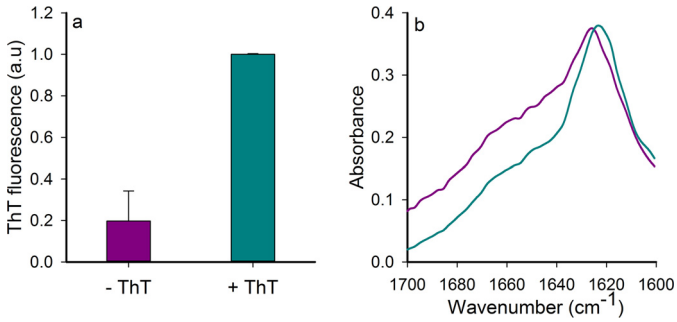

Figure 3. Binding of ThT to α-synuclein fibrils and the secondary structure of fibrils. *a*, 100 μM fibrils made in the absence and presence of 1 mM ThT were incubated with 1 mM ThT. After washing (see "Experimental procedures") the amount of ThT that remained bound to the fibrils was determined by measuring ThT fluorescence. The *error bars* represent the spread from two independent experiments. *b*, FTIR spectra of fibrils formed by 100 μM α-synuclein in the absence (*purple*) and presence (*cyan*) of ThT. The spectra were acquired at a time corresponding to three times the t_{50} of ThT fluorescence-monitored kinetics.

more, the nature of the fibrils formed depended not on the nature of the seed but on whether ThT was present or not during aggregation (data not shown).

Binding of ThT to fibrils and its effect on fibril secondary structure

To determine whether the fibrils made in the presence of ThT had ThT incorporated into their structure, 100 μM fibrils made in the presence and absence of ThT were incubated with the same concentration (1 mM) of ThT. Free and loosely bound ThT was then removed by washing the fibril pellet with buffer following centrifugation. ThT fluorescence was measured for equal concentrations of the fibrils to compare the extent of ThT bound to fibrils made in the absence and presence of ThT (Fig. 3*a*). The ThT fluorescence of fibrils made in the presence of ThT was about 5-fold higher than that of the fibrils made in the absence of ThT but to which ThT was subsequently added. Comparable results were obtained when the concentration of associated ThT was determined by measuring the absorbance at 412 nm (supplemental Fig. S3*a*) after first dissolving the fibrils in 8 M GdnHCl. Hence, ThT remained tightly bound to the fibrils made in its presence, presumably by intercalation inside the fibrils. These results suggested that the fibrils made in the absence and presence of 1 mM ThT differed in their structures.

To determine whether the fibrils made in the presence and absence of ThT differed in their secondary structures, infrared spectra were acquired (Fig. 3*b* and supplemental Fig. S3, *b* and *c*). The presence of the peak near 1630 cm^{-1} for both types of fibrils suggested that the fibrils had typical parallel β-sheet structures. This peak near 1630 cm^{-1} appeared at a lower wave number for the fibrils made in the presence of ThT compared with the fibrils made in the absence of ThT, which suggested an increase in the number of β-strands in the fibrils or a change in the twist angle of the β-sheet in fibrils made in the presence of ThT (54, 55).

Structural characterization of fibrils by hydrogen–deuterium exchange mass spectrometry

HDX-MS was used to further characterize the difference in the internal structures of the fibrils made in the absence and presence of 1 mM ThT. In HDX-MS studies, the amide hydrogen sites that are protected against HDX can be localized to specific segments of the protein sequence by proteolytic fragmentation at low pH after the HDX reaction is complete. A peptide map of α-synuclein, covering 100% of the sequence, was first generated by controlled proteolysis using pepsin at low pH (supplemental Fig. S4). The measured mass of each peptide was found to be the same as its calculated mass (supplemental Table S1), except for peptide 95–109 with a mass 18 daltons less than its calculated mass, probably due to water loss. A 5-min labeling pulse was given by incubating the fibrils as well as monomeric protein in deuterated buffer at pH 7.0, 25 °C. Control samples having no deuteration (0% D) and complete deuteration (95% D) were also run to calculate the amount of deuterium incorporation in different samples (supplemental Fig. S5). As expected for an intrinsically disordered protein, the monomeric protein showed complete labeling in all the sequence segments after 5 min of HDX (supplemental Fig. S6). Regions of the protein that are highly flexible or that remain unfolded in the fibrils would get labeled to the same extent as they do in the monomer. Regions that are part of the structural core of the fibrils would remain protected and not be labeled. In all fibrils obtained under the two differing conditions, the sequence segments spanning residues 39 to 94 were found to remain highly protected and unlabeled, whereas sequence segments spanning residues 95 to 140 were fully labeled (Fig. 4 and supplemental Fig. S5).

Interestingly, sequence segments spanning residues 1 to 38 showed bimodal mass distributions for the fibrils formed in the absence of ThT but highly protected unimodal mass distributions for the fibrils formed in the presence of 1 mM ThT (Fig. 4). The bimodal mass distributions for the sequence segments spanning residues 1 to 38 indicated the existence of two different conformations differing in structure in this region. One of the conformations showed protection against HDX and hence was structured, whereas the other conformation showed no protection against HDX and hence was not structured in the sequence segment 1–38. Taken together, the data presented in Fig. 4 show that fibrils formed in the absence of ThT existed in at least two conformations. One of the conformations had a structured core from residues 1 to 94, whereas the other conformation had a structured core only from residues 39 to 94 (Fig. 5, *a* and *b*). On the other hand, fibrils formed in the presence of 1 mM ThT had only a single conformation with a structured core from residues 1 to 94 (Fig. 5*c*).

Differences in molecular structures of fibrils with different morphologies

To correlate the structural core with external morphology for fibrils formed in the absence of ThT, the relative amounts of the two conformations were quantified by fitting the bimodal mass distributions obtained for sequence segments 1–17 and 18–38 to the sum of two Gaussian distributions (Fig. 6*a*). In addition, the fractions of helical and flat fibrils were quantified by counting the numbers of the two types of fibrils from AFM images (Fig. 6*a*). About 70% of the fibrils were found to be helical, and the remaining ~30% fibrils had a flat morphology. Interestingly, about 70% of the fibrillar protein molecules had a

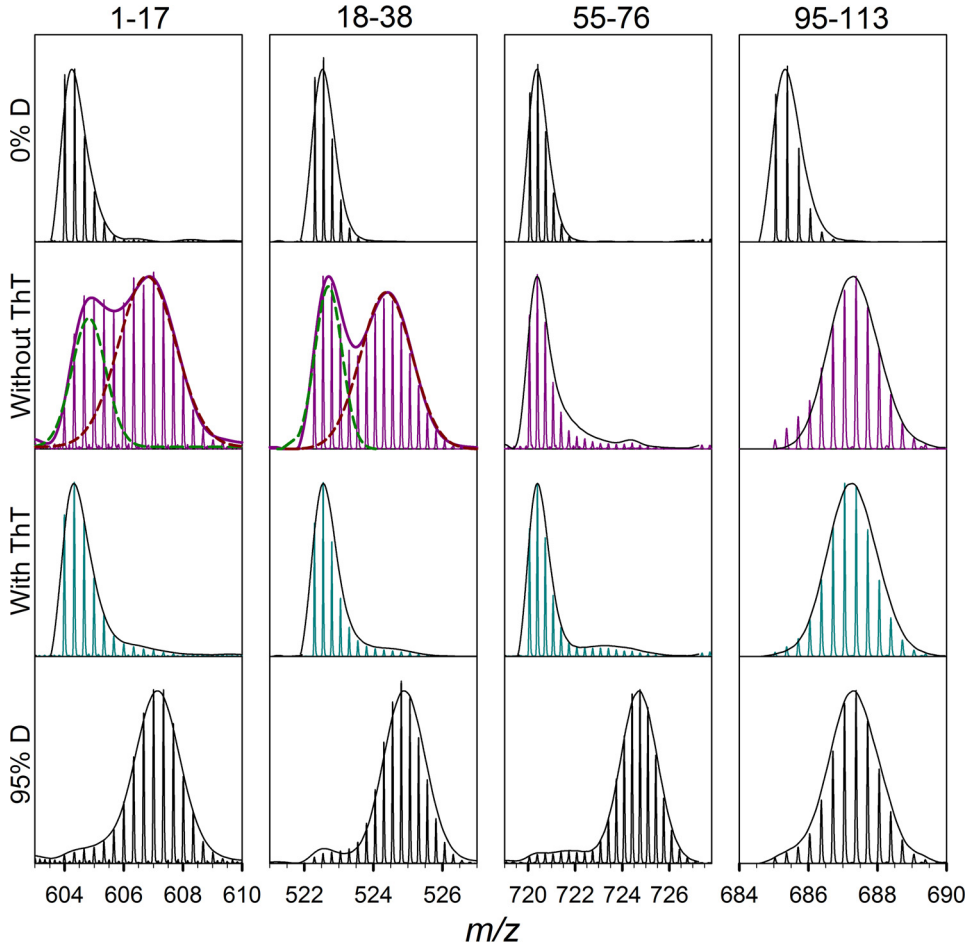

Figure 4. Conformational heterogeneity in fibrils formed by α-synuclein. Representative mass spectra of peptide fragments of α-synuclein for fibrils formed in the absence and presence of 1 mM ThT along with the mass spectra of protonated (0% D) and deuterated (95% D) controls. Peptide fragments corresponding to sequence segments 1–17 and 18–38 show bimodal mass distributions for fibrils formed in the absence of ThT and unimodal mass distributions for fibrils formed in the presence of 1 mM ThT.

structural core region extending from residues 39 to 94, whereas the remaining ~30% of the fibrillar protein molecules had a fibril core that extended from residues 1 to 94. These observations suggested that the helical fibrils are likely to have a core region extending from residues 39 to 94, whereas the flat, ribbon-like fibrils are likely to have a core region extending from residues 1 to 94. To further establish whether the flat, ribbon-like and helical fibrils had core regions extending from residues 1 to 94 and residues 39 to 94, respectively, the structural cores and morphologies of the fibrils were studied at 0.3 mM ThT instead of in the absence of ThT. Importantly, the AFM and HDX-MS studies showed that about 30% of the fibrils were helical in morphology and had a core region extending from residues 39 to 94, and about 70% of them were flat fibrils and had a core region extending from residues 1 to 94 (Fig. 6*b*). Hence, these data suggested that the helical fibrils had a core region extending from residues 39 to 94 and the flat fibrils had a core region extending from residues 1 to 94. These results also suggested that the average helical fibril and the average flat, ribbon-like fibril contained similar numbers of protein molecules.

The structure of the N-terminal region was found to differ in the two types of α-synuclein fibrils. In the ribbon-like fibrils, but not in the helical fibrils, the N-terminal region was found to be part of the structural core. This suggested that the N-terminal region plays an important role in determining the morphology of the fibrils. Helical fibrils formed in the absence of ThT did not convert into ribbon-like fibrils after incubating the fibrils in 1 mM ThT for 24 h at 25 °C (data not shown), suggesting that the fibrils have a stable structure and do not interconvert.

The presence of ThT modulated the fibrillar conformation, and it was important to determine how this occurred. To this end, α-synuclein aggregation reactions were carried out at different concentrations of ThT ranging from 0 to 1 mM, and AFM imaging was used to determine the relative fraction of helical fibrils formed at each concentration of ThT (Fig. 6*c*). We found that the relative fraction of helical fibrils decreased monotonically with an increase in the concentration of ThT present and that no helical fibrils had formed at 1 mM ThT concentration. The structure of the final aggregates was also determined using HDX-MS (supplemental Fig. S7). The relative amounts of the two fibrillar conformations were quantified by fitting the bimodal mass distributions obtained for the sequence segment 18–38 to the sum of multiple Gaussian distributions (supplemental Fig. S7). Interestingly, the relative amount of fibrillar

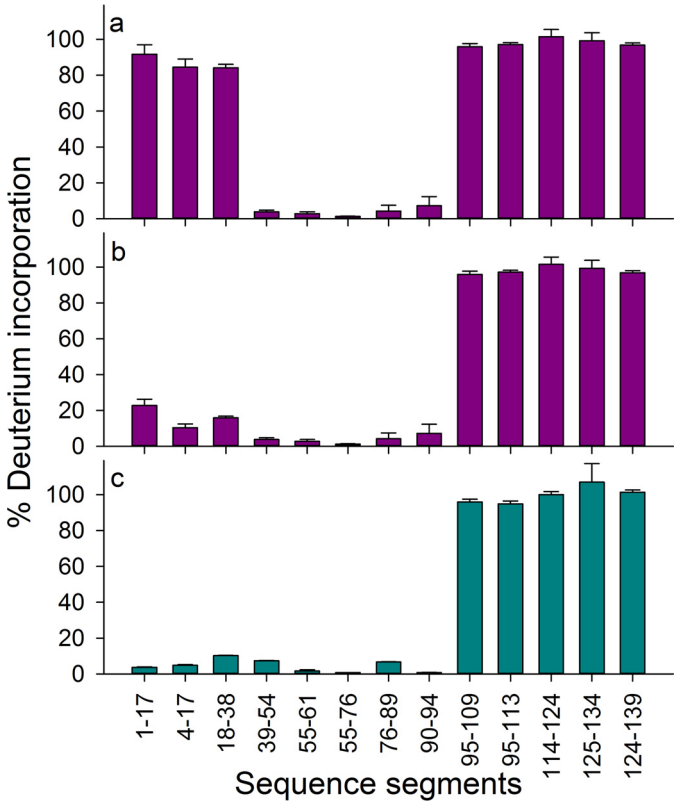

Figure 5. The structural core of the α-synuclein fibrils. *a–c*, the percent deuterium incorporation into different sequence segments of fibrils formed by α-synuclein in the absence (*a* and *b*) and presence (*c*) of 1 mM ThT. The deuterium incorporation data for sequence segments 1–17, 4–17, and 18–38 in *a* correspond to the higher mass distribution of the observed bimodal mass distribution, and the data for the same segments in *b* correspond to the lower mass distribution of the observed bimodal distribution. The data presented in *c* correspond to the unimodal mass distribution observed for the sequence segments for fibrils formed in the presence of 1 mM ThT. The *error bars* represent S.D. from three independent experiments.

protein with a core extending from residues 39 to 94 decreased with increasing concentration of ThT (Fig. 6*c* and supplemental Fig. S7). Thus, the relative amount of helical fibrils decreased from 70% when the fibrillation was carried out in the absence of ThT to 0% when fibrillation was carried out in the presence of 1 mM ThT. These results showed that ThT reduced structural heterogeneity in the fibrils formed by α-synuclein.

Monitoring the formation of α-synuclein oligomers during fibrillation

To determine whether oligomer formation occurred during the fibril formation reaction carried out in either the absence or presence of ThT, α-synuclein was incubated at two different concentrations (100 and 690 μM (10 mg/ml)) under the fibrillation conditions (pH 7.0 and 37 °C) for 5 h. Size-exclusion chromatography was used to detect whether oligomers had formed. Oligomers were not observed to have formed in either the absence or presence of ThT (supplemental Fig. S8, *a* and *b*). Oligomers could only be observed (supplemental Fig. S8*c*) when aggregation was carried out at high a protein concentration (10 mg/ml) in a different (PBS) buffer at pH 7.4 and 37 °C for 5 h, as described previously (31).

Characterization of the toxicity levels of the fibrils

To determine whether the fibrils with different structures were differentially toxic to cells, the toxicities of the fibrils formed in the absence and presence of 1 mM ThT were measured using HEK-293T cells (human embryonic kidney cells). Equal amounts of fibrils (2.5 μM) were incubated with HEK-293T cells for 24 h, and toxicity was measured using the Wst-1 assay (Fig. 7). To eliminate the effect of any free ThT, the fibrils were first washed multiple times with Milli-Q water to remove any free and loosely bound ThT. For toxicity assays, 1 μM ThT was used as a buffer control, and cells without the addition of any buffer served as the control. It was found that about 113 ± 22% of the cells were viable after incubating them with fibrils formed in the absence of ThT, whereas about 76 ± 8% of the cells were viable in the case of fibrils formed in the presence of ThT. It could be concluded that the flat, ribbon-like fibrils formed in the presence of ThT were significantly more toxic to the cells than the fibrils formed in the absence of ThT. It would therefore appear that fibrils with a flat, ribbon-like morphology are more toxic than fibrils with a helical morphology. Control experiments were carried out to ensure that the observed toxicity was due to fibrils and not to any free (unbound) ThT. To this end, toxicity assays were carried out at various free ThT concentrations (supplemental Fig. S9). Free ThT was found to be toxic to cells at concentrations greater than 1 μM (supplemental Fig. S9) but not at lower concentrations.

Discussion

The current study was focused on understanding the structural and mechanistic basis for heterogeneity in α-synuclein fibrils and its modulation by the small molecule ThT. In the case of several neurodegenerative diseases, the aggregating protein concerned has been found to adopt distinct fibrillar conformations (5, 8, 15, 19). Thus, understanding the structural and physical basis for fibril heterogeneity may shed light on the different pathological behaviors of distinct fibrillar conformations.

Structural heterogeneity in α-synuclein fibrils and their toxicity levels

In this study, both helical and flat, ribbon-like fibrils were found to form under the same aggregation conditions (Fig. 2, *a* and *c*). In previous studies as well, α-synuclein was found to form two types of fibrils, under particular aggregation conditions, which differed in their secondary structures, morphologies, folds, and the extent and distribution of β-sheets but had the same structural core encompassing residues 38–95 (12, 13). In contrast, the two types of fibrils observed to form together in the current study had different structural cores (Fig. 5, *a* and *b*). The structural core of the helical fibrils comprises residues 39–94, and that of the flat, ribbon-like fibrils comprises residues 1–94 (Fig. 5, *a* and *b*). Multiple studies using solid-state NMR (10, 12, 32–34), HDX-MS (31, 35), HDX-NMR (13, 33), EPR spectroscopy (36, 37), and proteinase K treatment (38) have previously identified the structural core of the α-synuclein fibrils. Most of the studies have determined that residues 31–109 form the structural core of the α-synuclein fibrils (10,

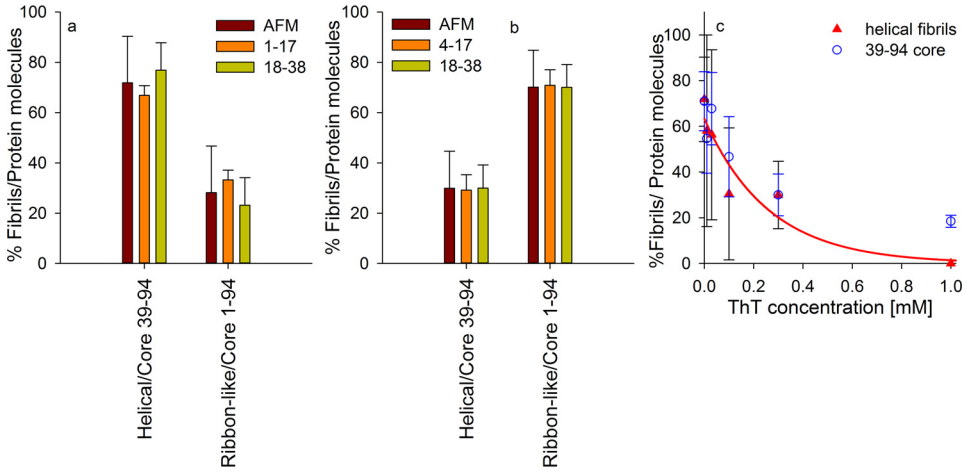

Figure 6. Quantification of the two types of fibrils formed by α-synuclein. *a*, shows data for fibrils formed in the absence of ThT. *b*, shows data for fibrils formed in the presence of 0.3 mM ThT. The *brown bars* represent the percentages of fibrils that were helical and ribbon-like, as determined from counting the fibrils seen in the AFM images. The percentages of protein molecules in fibrils that had and did not have a structural core extending down to residue 1 were determined from the bimodal mass distributions seen for sequence segments 1–17 (*orange*) and 18–38 (*green*) as described in the legend for Fig. 4. The percentage of fibrillar protein molecules with a core extending down to residue 1 matches the percentage of flat, ribbon-like fibrils formed in both the absence (*a*) and presence (*b*) of 0.3 mM ThT. *c*, shows the percentages of fibrillar protein molecules with a core extending from residues 39 to 94, formed at various ThT concentrations, as quantified from the higher mass peak of the mass distributions of sequence segment 18–38 (supplemental Fig. S7). Also shown are the percentages of helical fibrils formed at various ThT concentrations, determined by counting the two types of fibrils seen in AFM images. The *red line* through the plot of % helical fibril data is described as 63 exp(−3.8 [ThT]). The *error bars* represent S.D. from three independent experiments.

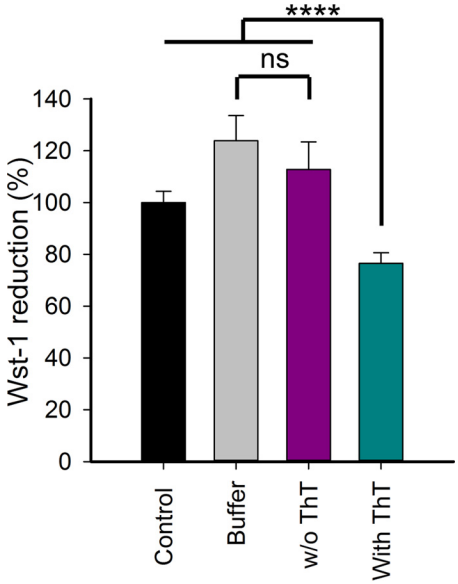

Figure 7. Cytotoxicity of α-synuclein fibrils. The cytotoxicity of α-synuclein fibrils (2.5 μM) to HEK-293T cells was measured using water-soluble tetrazolium (Wst-1 assay kit). Fibrils were made by incubating 100 μM α-synuclein at 37 °C in the absence and presence of 1 mM ThT. Fibrils were added to a final concentration of 2.5 μM to the cells in each well. The concentration of ThT associated with 2.5 μM fibrils was ~0.25 μM. After incubating the cells for 24 h, Wst-1 reagent was added to the wells. After incubating them for 2.5 h, the OD at 477 nm was measured. Absorbance data were normalized to that of the untreated cells (*Control*) having 100% cell viability (*ns* = non-significant; ****, $p < 0.0001$ using an unpaired *t* test). *Buffer* represents cells treated with only 1 μM ThT as described under "Experimental procedures." The *error bars* represent S.E. from five independent experiments, each with three replicates.

12, 13, 15, 31–38). In a previous study, ribbon-like fibrils were found to form under one aggregation condition and cylindrical fibrils under another aggregation condition, with the two types also differing in their morphology, structural core, toxicity, and infectivity (10). The cylindrical fibrils observed in that study resembled the helical fibrils observed in the current study in having a structural core composed of residues 39–94; and the ribbon-like fibrils observed in that study were similar to the ribbon-like fibrils observed in the current study in having a structural core formed by residues 1–94 (10). Although the structurally distinct fibrils were shown to differ in their toxicity potentials (10), the properties of the fibrils that determine their toxicity potentials are not well-known. The factors that are likely to affect the toxicity of fibrils include their stability, their ability to interact with membranes, and their surface hydrophobicity (20–22).

The flat, ribbon-like fibrils, which possess the extended structural core, are somewhat more toxic than the helical fibrils (Fig. 7). Interestingly, in a previous study, fibrils formed by peptides of two different lengths, which were derived from the α-synuclein NACore (segment 68–78) and subNAC (segment 69–77) regions, which differed in their structural core, were also found to differ in their cytotoxicity (39). Fibrils made of the longer peptide (NACore), which had a longer structural core, were more cytotoxic than those made by the shorter peptide (39). Further studies are required to delineate the biological importance of the length of the amyloid core.

It is interesting to note that although the fibrils formed in the absence of ThT include flat ribbon-like fibrils similar to those formed in the presence of ThT, which are toxic, little if any toxicity was observed for them. It seems that this might be due to the relatively low proportion of ribbon-like fibrils formed in the absence of ThT.

It should be noted that in this study, toxicity was measured after the addition of the fibrils to cells for 24 h. It is possible that during this incubation with the cells, the fibrils break down into smaller aggregates and that it is these smaller aggregates that are toxic. In this context, it should also be noted that oligomers and prefibrillar aggregates formed by α-synuclein are reported to be toxic (56–60) as are fibrils (10, 61, 62).

Thioflavin T modulates fibrillar heterogeneity

Different internal structures lead to different external fibril morphologies

Different fibril morphologies can originate from distinct molecular structures or from different arrangements of the same molecular structure (6). In the current study, α-synuclein fibrils possessing different morphologies were found to comprise internal structural cores of different lengths. It is likely that the fibrils differing in the length of the structural core also differ in extent and organization of β-sheets. The observation that the flat, ribbon-like fibrils with an extended structural core had a larger diameter/height than the helical fibrils (Fig. 2, *c* and *d*) suggests that they are likely to have a higher fold symmetry than the helical fibrils, as observed previously for Aβ fibrils (6). In the case of the small protein barstar as well, fibrils of very different morphology and diameter, which were, however, formed under different solution conditions, were found to have inner structural cores of different lengths (63, 64). At present, the link between a short structural core and helical fibrillar morphology, and between a longer structural core and flat, ribbon-like fibrillar morphology is not understood in the case of α-synuclein.

Origin of α-synuclein fibril heterogeneity and its reduction by ThT

Structural heterogeneity in α-synuclein fibrils could arise from heterogeneity at the monomer level, which would lead to the formation of distinct nuclei. Because of its intrinsically disordered nature, α-synuclein can adopt various conformations in a given solution condition as characterized by electrospray ionization mass spectrometry (65), single-molecule AFM (66), and NMR (67). Modifications in the amino acid sequence and solution conditions have been shown to modulate the conformational composition of the ensemble of α-synuclein molecules (66). The conformational diversity could determine the relative proportion of different aggregates that can be formed, as suggested previously for other proteins (23). It can then be expected that the stabilization of a specific conformational state upon binding to a small molecule might lead to the formation of specific aggregates.

Structural heterogeneity in α-synuclein fibrils could also arise from the utilization of multiple pathways for fibril formation. For several other proteins, including barstar (64, 68) and the mouse prion protein (70), structurally distinct amyloid fibrils have been shown to form on different aggregation pathways under different aggregation conditions. In the case of α-synuclein, morphologically and structurally different aggregates have been shown to form from structurally distinct oligomers (31). One oligomer was found to be on pathway to fibril formation and had a structural core similar to that of fibrils, and the other oligomer with a different structural core grew into amorphous aggregates (31). In the current study, the inability to detect the formation of oligomers during fibril formation under the aggregation conditions used, either in the absence or presence of ThT (see "Results" and supplemental Fig. S8), did not permit us to determine whether the ribbon-like and helical fibrils arose from structurally distinct oligomers formed on different pathways of fibril formation.

The formation of distinct α-synuclein fibrils suggests that multiple nucleation events can take place under the same aggregation condition. Changes in the aggregation condition may affect the nucleation rate and elongation rate differently for distinct nuclei, which would play an important role in modulating structural heterogeneity. In the current study, the observation that the presence of ThT accelerates nucleation and elongation (Fig. 1) suggests that ThT binds to early species formed during the fibrillation of α-synuclein. Binding of ThT to early aggregates on one pathway, when multiple pathways are operative, will stabilize those aggregates and result in a reduction in fibril heterogeneity.

Role of ThT in modulating the fibril formation reaction of α-synuclein

ThT is known to bind to cross-β-sheet structures found in amyloid fibrils and has been used widely to monitor the amyloid fibril formation reaction of many proteins (50). The binding of ThT to fibrils can occur in different ways. ThT can bind perpendicular to the long fibril axis in the cavities formed by the side chains of aromatic/hydrophobic residues across consecutive β-strands on the surface of the β-sheet in the fibrils (51, 71–73). ThT is also known to bind in a parallel orientation to the peptide strand (74). It also appears that ThT can bind to the peptide backbone via π-π interactions (75). Hence, it is not surprising that ThT can bind diverse types of amyloid fibrils with different affinities (51). If fibrillar structures (nuclei), which form very early, differ in their binding affinity for ThT, then the early structure (nucleus) that binds most tightly to ThT will be stabilized and, hence, populated the most. The relative amounts of different fibrils formed will reflect the relative amounts of the initial aggregates (nuclei). Hence, the relative amounts of different fibrils that form will depend on the concentration and binding affinity of the ThT present. Thus, ThT must bind strongly to the early fibrillar structures (nuclei) that lead to the formation of the flat, ribbon-like fibrils. In fact, ThT is seen to remain bound to the final, mature, flat, ribbon-like fibrils (Fig. 3*a*).

The observation that ThT accelerates the fibrillation of α-synuclein by increasing the nucleation rate (as indicated in the reduction of the lag phase) (Fig. 1) suggests that ThT does indeed bind to early structures (nuclei) formed during the fibrillation process, resulting in an increase in the nucleus concentration and the elongation rate. In the case of Aβ, a previous study shows that the nucleation rate is affected more than the elongation rate in the presence of ThT, which also suggests that ThT binds to the early structures on the fibrillation pathway (52, 76).

It is also possible that ThT accelerates the amyloid fibril formation reaction by binding to monomer. In the case of α-synuclein, the electrostatic interaction of ThT with monomeric α-synuclein might favor nucleation or the conformation conversion of monomer to aggregation-prone structures that ultimately form the nucleus. Indeed, ThT is known to bind to the negatively charged C terminus of monomeric α-synuclein (53). Nevertheless, fibrils made from α-synuclein truncated at its C terminus can still bind ThT (77), indicating that ThT binds differently to monomer and to fibril.

The C terminus is known to be the most solvent-exposed region in both oligomers (31, 78, 79) and fibrils (10, 12, 13, 15, 31–38). The C terminus is also known to stabilize the disordered conformation of the protein by interacting with the N terminus or NAC domain (80–83). It is likely that the interaction of the C terminus with the N-terminal region suppresses the participation of the latter in forming the structural core of amyloid fibrils (53). Not surprisingly, then, C-terminal truncation significantly accelerates the fibrillation of α-synuclein (77, 84). Binding of the C-terminal domain to the NAC region protects the NAC region from participating in aggregation. Binding of the C terminus to other proteins (85), polyamines (86, 87), and metal ions (9, 88) increases the rate of fibril formation, suggesting that neutralization of the negatively charged C terminus prevents its binding to the NAC region and the N terminus of the protein. Thus, the interaction of ThT with the C terminus of α-synuclein may play an important role in modulating the fibrillation reaction.

It should be noted that, in this study, a range of ThT concentrations was used to investigate the effect of ThT in modulating structural heterogeneity in α-synuclein fibrils (Fig. 6). It was found that fibril formation by α-synuclein was not modulated at ThT concentrations below 30 μM, a concentration known to be the critical micelle concentration for ThT (89). It seems therefore that structural modulation by ThT during fibril formation, as seen in this study, is effected by micellar ThT. ThT is used widely to monitor fibril formation reactions, and the present study suggests that it is safe to do so at concentrations below its critical micelle concentration.

In summary, the small molecule ThT has been shown to modulate the fibril formation reaction of α-synuclein and to thereby modulate the structural heterogeneity of the fibrils that form. The presence of ThT during the fibril formation favors the formation of flat, ribbon-like fibrils over the formation of helical fibrils. The flat, ribbon-like fibrils have inner structural core extending from residues 1 to 94, whereas the helical fibrils have an inner structural core extending from residues 39 to 94. The current study highlights the potential use of small molecules in modulating the fibril formation reaction of proteins so that the less toxic aggregates are favored over the more toxic aggregates.

Experimental procedures

Protein expression and purification

The plasmid pRK172 containing the human α-synuclein gene was a kind gift from Prof. A. L. Fink. The protein was expressed and purified as described previously (90) with some modification to the procedure. *Escherichia coli* BL21(DE3) codon plus (Stratagene) cells transformed with pRK172 were grown overnight at 37 °C in LB medium containing 100 μg/ml ampicillin and then subcultured into 1000 ml of LB containing 100 μg/ml ampicillin. At an OD_{600} of 0.8–1.0, the cells were induced by adding IPTG at a final concentration of 10 μg/ml and pelleted down after 5 h. They were resuspended in osmotic shock buffer (30 mM Tris-HCl, 40% w/v sucrose, 2 mM EDTA, pH 7.2), incubated at 25 °C for 15 min, and centrifuged to remove supernatant. The pellet was resuspended in Milli-Q water containing about 1 mM $MgCl_2$, and the supernatant was obtained after centrifugation. This supernatant was dialyzed twice against 20 mM Tris-HCl buffer, pH 8.0, at 4 °C. The protein was denatured by adding 8 M urea solution and loaded onto a DEAE FF ion-exchange column (5 ml, HiTrap, GE Healthcare). The loaded protein was washed and then eluted out using a gradient of 100–300 mM NaCl. The eluted protein was concentrated by ultrafiltration (Millipore), flash-frozen in liquid N_2, and stored at −80 °C.

Chemicals, buffers, and aggregation condition

All of the reagents used were of the highest purity grade available from Sigma-Aldrich unless specified otherwise. GdnHCl was procured from USB Corp. The stored protein was concentrated by filtration using a YM3 filter (Millipore) and denatured in 6 M GdnHCl before injecting it into a size-exclusion column (Superdex 200 10/300 GL). The protein was eluted out in 20 mM sodium phosphate, 0.01% sodium azide, and 0.1 mM EDTA, pH 7.0 (aggregation buffer) and passed through a YM100 filter to remove any aggregated protein. For aggregation reactions, 500 μl of 100 μM protein was agitated at 750 rpm and 37 °C (Eppendorf ThermoMixer) in a 1.5-ml centrifuge tube. For aggregation reactions in the presence of ThT, 500 μl of 100 μM protein solution containing 0.01 to 1 mM ThT was agitated at 750 rpm and 37 °C.

Aggregation studies

Aliquots were withdrawn from the aggregation reaction at various time points, and the amount of fibrils was monitored by measuring the ThT fluorescence at pH 8.0 in 20 mM Tris-HCl buffer. In the assay, 10 μM ThT and 1 μM protein were used. For aggregation reactions carried out in the absence of ThT, 5-μl aliquots were withdrawn and mixed with 495 μl of 20 mM Tris-HCl buffer containing 10 μM ThT. For aggregation reactions carried out in the presence of 1 mM ThT, 5-μl aliquots were withdrawn and mixed with 495 μl of 20 mM Tris-HCl buffer. Then fluorescence was monitored using a Fluoromax-4 spectrofluorometer with the excitation and emission wavelengths set at 440 and 482 nm, respectively.

Quantification of ThT bound to α-synuclein fibrils

To 45 μl of 100 μM fibrils prepared in the absence of ThT, 4.5 μl of 10 mM ThT was added. To 45 μl of 100 μM fibrils prepared in the presence of 1 mM ThT, 4.5 μl of Milli-Q water was added. In both cases, the fibrils were then incubated at 25 °C for 90 min and then spun down at 20,000 × *g* for 10 min at 9 °C. The pellet was resuspended in 50 μl of aggregation buffer (without ThT). This was repeated four times to remove the free/loosely bound ThT. Fibril concentration was determined using the BCA assay kit (Thermo Scientific), and equal amounts of fibrils formed in the absence and presence of ThT were used to monitor the ThT fluorescence and compare the amount of ThT retained in each fibril sample. The amount of ThT bound to the fibrils was also measured by dissolving the fibrils in 8 M GdnHCl and monitoring the absorbance at 412 nm.

Atomic force microscopy

50 μl of fibrils applied onto freshly cleaved mica were incubated for 3 min. The mica surface was rinsed twice with filtered

Milli-Q water and dried under vacuum for 45–60 min. The AFM images were acquired using a FastScan Bio (Bruker) instrument and analyzed using WSxM software. The height distribution of the fibrils was obtained by measuring the heights of about 200 fibrils from 10 images of fibrils formed in the presence of ThT and about 1000 fibrils from 36 images of fibrils formed in the absence of ThT. The nature of the periodicity seen in the helical fibrils was determined by measuring 32 fibrils from nine images.

Fourier transform infrared (FTIR) spectroscopy

For FTIR measurements, samples were spun down at 20,000 × *g* for 10 min at 9 °C, and fibrils were washed three times with aggregation buffer (without EDTA) made in D_2O and then resuspended in the same buffer. A thin film was prepared on the diamond crystal by drying 3 μl of sample using N_2 gas. FTIR spectra were acquired using a Thermo Nicolet 6700 FT-IR spectrometer. The FTIR spectra of the fibrils were analyzed after background subtraction of the spectrum of the appropriate aggregation buffer.

Peptide mapping

To generate a peptide map of α-synuclein, the protein, dissolved in water, was subjected to online pepsin digestion in 0.05% formic acid using an immobilized pepsin cartridge (Applied Biosystems) at a flow rate of 50 μl/min on a nanoAcquity UPLC (Waters). The eluted peptides were collected using a peptide trap column (C18 reversed-phase chromatography column), and eluted into an analytical C18 reversed-phase chromatography column using a gradient of 3–40% acetonitrile (0.1% formic acid) at a flow rate of 45 μl/min. The peptides were directed to the coupled Synapt G2 HD mass spectrometer (Waters). The peptides were sequenced using the MS/tandem MS (MS^E) method followed by analysis with ProteinLynx Global Server software (Waters) and manual inspection.

HDX-MS measurements

Fibrils were prepared as described above. 80 μl of 100 μM fibrils were spun down at 20,000 × *g* for 20 min at 9 °C. The pellet was resuspended in 20 μl of aggregation buffer. To initiate deuterium labeling, 10 μl of the above sample was diluted into 190 μl of aggregation buffer (without EDTA) made in D_2O and incubated at 25 °C for 5 min. After a 5-min pulse, 200 μl of the above sample was mixed with 400 μl of ice-cold quench buffer (0.1 M glycine-HCl, 8.4 M GdnHCl, pH 2.5) and incubated for 1 min on ice to dissolve the fibrils. The samples were desalted using a Sephadex G-25 HiTrap desalting column equilibrated with water at pH 2.5 and Akta Basic HPLC. The desalted samples were injected into the HDX module coupled with a nanoACQUITY UPLC system (Waters) for online pepsin digestion using an immobilized pepsin cartridge (Applied Biosystems). Further processing of the sample for mass determination using a Waters Synapt G2 mass spectrometer was carried out as described previously (91).

Peptide masses were calculated from the centroid of the isotopic envelope using MassLynx software, and the shift in the mass of labeled peptide relative to the unlabeled peptide was used to determine the extent of deuterium incorporation. As the sample was in 95% D_2O during labeling and was exposed to H_2O after dissolution in GdnHCl, control experiments were carried out to correct for back-exchange and forward-exchange. To this end, monomeric α-synuclein was completely deuterated by incubating it in 20 mM sodium phosphate buffer, pH 7.0 (95% D_2O) at 25 °C for 5 min. The fully deuterated α-synuclein sample was then processed in exactly the same way as the aggregates. The extent of deuterium incorporation in each peptide, % D, was determined using the following equation,

$$\%\ D = (m(t) - m(0\%))/(m(95\%) - m(0\%)) \times 100 \quad \text{(Eq. 1)}$$

where $m(t)$ is the measured centroid mass of the peptide at time point t, $m(0\%)$ is the measured mass of an undeuterated reference sample, and $m(95\%)$ is the measured mass of a fully deuterated reference sample (in 95% D_2O) (69).

The percent deuterium incorporation for peptides showing a bimodal distribution was calculated as described previously (14, 91). The centroid mass for each peak was obtained by fitting the bimodal mass distributions to the sum of two Gaussian distributions using OriginPro 8. The % D for each peak was determined using Equation 1.

Cytotoxicity assay

Equal concentrations (1 mM) of ThT were added to the fibrils made under the two different conditions, and the fibrils were incubated at 25 °C for 15 min. The fibrils were spun down at 20,000 × *g* for 20 min at 9 °C, the supernatant was removed, and the fibrils were washed with an equal volume of autoclaved Milli-Q water. The washing process was repeated three times, and then the fibrils were resuspended in autoclaved Milli-Q water. The concentration of the fibrils was determined using the BCA assay after dissolving the fibrils in 4 M GdnHCl. Equal concentrations (2.5 μM) of fibrils made under the two different conditions were used for the cytotoxicity experiments. Autoclaved Milli-Q water containing 1 μM ThT was used as a buffer control in the cytotoxicity assay. For the assay, HEK-293T cells (ATCC) were cultured in DMEM (Gibco) supplemented with 10% FBS at 37 °C in a 5% CO_2-humidified environment. Cells were plated in a 96-well plate at a density of 5000 cells/well to a final volume of 100 μl. After incubation for 25 h, 10 μl of fibrils (25 μM) or ThT only (0.1–5 μM) was added to each well, and the cells were further incubated for 24 h at 37 °C in 5% CO_2. The Wst-1 assay kit (Roche) was used to measure the viability of the cells. 9 μl of Wst-1 reagent was added into each well, and the cells were incubated for 2.5 h at 37 °C in 5% CO_2. The optical density at 477 nm was measured with a microplate reader (SpectraMax M5). Data were normalized with respect to the data obtained with untreated (control) cells.

Author contributions—H. K., J. S., J. B. U., and P. K. designed the experiments. H. K. performed the experiments. H. K., J. S., and J. B. U. analyzed the results and wrote the manuscript. The final version of the manuscript was approved by all of the authors.

Acknowledgments—We thank the members of our laboratory for discussion and for comments on the manuscript. We thank Sahil Lall for assistance in carrying out the cytotoxicity experiments in the laboratory of M. K. Mathew. The AFM images were collected at the Central Imaging Facility of the National Centre for Biological Sciences.

References

1. Spillantini, M. G., Schmidt, M. L., Lee, V. M., Trojanowski, J. Q., Jakes, R., and Goedert, M. (1997) α-Synuclein in Lewy bodies. *Nature* **388,** 839–840
2. Goedert, M. (2001) α-Synuclein and neurodegenerative diseases. *Nat. Rev. Neurosci.* **2,** 492–501
3. Stefani, M., and Dobson, C. M. (2003) Protein aggregation and aggregate toxicity: New insights into protein folding, misfolding diseases and biological evolution. *J. Mol. Med.* (*Berl.*) **81,** 678–699
4. Singh, J., and Udgaonkar, J. B. (2015) Molecular mechanism of the misfolding and oligomerization of the prion protein: Current understanding and its implications. *Biochemistry* **54,** 4431–4442
5. Petkova, A. T., Leapman, R. D., Guo, Z., Yau, W. M., Mattson, M. P., and Tycko, R. (2005) Self-propagating, molecular-level polymorphism in Alzheimer's β-amyloid fibrils. *Science* **307,** 262–265
6. Paravastu, A. K., Leapman, R. D., Yau, W. M., and Tycko, R. (2008) Molecular structural basis for polymorphism in Alzheimer's β-amyloid fibrils. *Proc. Natl. Acad. Sci. U.S.A.* **105,** 18349–18354
7. Fitzpatrick, A. W., Debelouchina, G. T., Bayro, M. J., Clare, D. K., Caporini, M. A., Bajaj, V. S., Jaroniec, C. P., Wang, L., Ladizhansky, V., Müller, S. A., MacPhee, C. E., Waudby, C. A., Mott, H. R., De Simone, A., Knowles, T. P., *et al*. (2013) Atomic structure and hierarchical assembly of a cross-β amyloid fibril. *Proc. Natl. Acad. Sci. U.S.A.* **110,** 5468–5473
8. Lu, J. X., Qiang, W., Yau, W. M., Schwieters, C. D., Meredith, S. C., and Tycko, R. (2013) Molecular structure of β-amyloid fibrils in Alzheimer's disease brain tissue. *Cell* **154,** 1257–1268
9. Hoyer, W., Antony, T., Cherny, D., Heim, G., Jovin, T. M., and Subramaniam, V. (2002) Dependence of α-synuclein aggregate morphology on solution conditions. *J. Mol. Biol.* **322,** 383–393
10. Bousset, L., Pieri, L., Ruiz-Arlandis, G., Gath, J., Jensen, P. H., Habenstein, B., Madiona, K., Olieric, V., Böckmann, A., Meier, B. H., and Melki, R. (2013) Structural and functional characterization of two α-synuclein strains. *Nat. Commun.* **4,** 2575
11. Fändrich, M., Wulff, M., Pedersen, J. S., and Otzen, D. (2013) Fibrillar polymorphism, in. *Amyloid Fibrils and Prefibrillar Aggregates: Molecular and Biological Properties* (Otzen, D., ed), pp. 321–343, Wiley-VCH Verlag GmbH & Co. KGaA, Weinheim, Germany
12. Heise, H., Hoyer, W., Becker, S., Andronesi, O. C., Riedel, D., and Baldus, M. (2005) Molecular-level secondary structure, polymorphism, and dynamics of full-length α-synuclein fibrils studied by solid-state NMR. *Proc. Natl. Acad. Sci. U.S.A.* **102,** 15871–15876
13. Vilar, M., Chou, H. T., Lührs, T., Maji, S. K., Riek-Loher, D., Verel, R., Manning, G., Stahlberg, H., and Riek, R. (2008) The fold of α-synuclein fibrils. *Proc. Natl. Acad. Sci. U.S.A.* **105,** 8637–8642
14. Singh, J., and Udgaonkar, J. B. (2013) Dissection of conformational conversion events during prion amyloid fibril formation using hydrogen exchange and mass spectrometry. *J. Mol. Biol.* **425,** 3510–3521
15. Dearborn, A. D., Wall, J. S., Cheng, N., Heymann, J. B., Kajava, A. V., Varkey, J., Langen, R., and Steven, A. C. (2016) α-Synuclein amyloid fibrils with two entwined, asymmetrically associated protofibrils. *J. Biol. Chem.* **291,** 2310–2318
16. Bessen, R. A., and Marsh, R. F. (1994) Distinct PrP properties suggest the molecular basis of strain variation in transmissible mink encephalopathy. *J. Virol.* **68,** 7859–7868
17. Safar, J., Wille, H., Itri, V., Groth, D., Serban, H., Torchia, M., Cohen, F. E., and Prusiner, S. B. (1998) Eight prion strains have PrP(Sc) molecules with different conformations. *Nat. Med.* **4,** 1157–1165
18. Stöhr, J., Watts, J. C., Mensinger, Z. L., Oehler, A., Grillo, S. K., DeArmond, S. J., Prusiner, S. B., and Giles, K. (2012) Purified and synthetic Alzheimer's amyloid beta (Aβ) prions. *Proc. Natl. Acad. Sci. U.S.A.* **109,** 11025–11030
19. Qiang, W., Yau, W. M., Lu, J. X., Collinge, J., and Tycko, R. (2017) Structural variation in amyloid-β fibrils from Alzheimer's disease clinical subtypes. *Nature* **541,** 217–221
20. Butterfield, S. M., and Lashuel, H. A. (2010) Amyloidogenic protein-membrane interactions: Mechanistic insight from model systems. *Angew. Chem. Int. Ed. Engl.* **49,** 5628–5654
21. Xue, W. F., Hellewell, A. L., Hewitt, E. W., and Radford, S. E. (2010) Fibril fragmentation in amyloid assembly and cytotoxicity: When size matters. *Prion* **4,** 20–25
22. Marshall, K. E., Marchante, R., Xue, W. F., and Serpell, L. C. (2014) The relationship between amyloid structure and cytotoxicity. *Prion* **8,** 28860
23. Tanaka, M., and Komi, Y. (2015) Layers of structure and function in protein aggregation. *Nat. Chem. Biol.* **11,** 373–377
24. Jao, C. C., Hegde, B. G., Chen, J., Haworth, I. S., and Langen, R. (2008) Structure of membrane-bound α-synuclein from site-directed spin labeling and computational refinement. *Proc. Natl. Acad. Sci. U.S.A.* **105,** 19666–19671
25. Fauvet, B., Mbefo, M. K., Fares, M. B., Desobry, C., Michael, S., Ardah, M. T., Tsika, E., Coune, P., Prudent, M., Lion, N., Eliezer, D., Moore, D. J., Schneider, B., Aebischer, P., El-Agnaf, O. M., *et al*. (2012) α-Synuclein in central nervous system and from erythrocytes, mammalian cells, and *Escherichia coli* exists predominantly as disordered monomer. *J. Biol. Chem.* **287,** 15345–15364
26. Lashuel, H. A., Overk, C. R., Oueslati, A., and Masliah, E. (2013) The many faces of α-synuclein: From structure and toxicity to therapeutic target. *Nat. Rev. Neurosci.* **14,** 38–48
27. Davidson, W. S., Jonas, A., Clayton, D. F., and George, J. M. (1998) Stabilization of α-synuclein secondary structure upon binding to synthetic membranes. *J. Biol. Chem.* **273,** 9443–9449
28. Mirecka, E. A., Shaykhalishahi, H., Gauhar, A., Akgül, Ş., Lecher, J., Willbold, D., Stoldt, M., and Hoyer, W. (2014) Sequestration of a β-hairpin for control of α-synuclein aggregation. *Angew. Chem. Int. Ed. Engl.* **53,** 4227–30
29. Cabin, D. E., Shimazu, K., Murphy, D., Cole, N. B., Gottschalk, W., McIlwain, K. L., Orrison, B., Chen, A., Ellis, C. E., Paylor, R., Lu, B., and Nussbaum, R. L. (2002) Synaptic vesicle depletion correlates with attenuated synaptic responses to prolonged repetitive stimulation in mice lacking α-synuclein. *J. Neurosci.* **22,** 8797–8807
30. Lorenzen, N., Nielsen, S. B., Buell, A. K., Kaspersen, J. D., Arosio, P., Vad, B. S., Paslawski, W., Christiansen, G., Valnickova-Hansen, Z., Andreasen, M., Enghild, J. J., Pedersen, J. S., Dobson, C. M., Knowles, T. P., and Otzen, D. E. (2014) The role of stable α-synuclein oligomers in the molecular events underlying amyloid formation. *J. Am. Chem. Soc.* **136,** 3859–3868
31. Paslawski, W., Mysling, S., Thomsen, K., Jørgensen, T. J., and Otzen, D. E. (2014) Co-existence of two different α-synuclein oligomers with different core structures determined by hydrogen/deuterium exchange mass spectrometry. *Angew. Chem. Int. Ed. Engl.* **53,** 7560–7563
32. Tuttle, M. D., Comellas, G., Nieuwkoop, A. J., Covell, D. J., Berthold, D. A., Kloepper, K. D., Courtney, J. M., Kim, J. K., Barclay, A. M., Kendall, A., Wan, W., Stubbs, G., Schwieters, C. D., Lee, V. M., George, J. M., and Rienstra, C. M. (2016) Solid-state NMR structure of a pathogenic fibril of full-length human α-synuclein. *Nat. Struct. Mol. Biol.* **23,** 409–415
33. Cho, M. K., Kim, H. Y., Fernandez, C. O., Becker, S., and Zweckstetter, M. (2011) Conserved core of amyloid fibrils of wild type and A30P mutant α-synuclein. *Protein Sci.* **20,** 387–395
34. Heise, H., Celej, M. S., Becker, S., Riedel, D., Pelah, A., Kumar, A., Jovin, T. M., and Baldus, M. (2008) Solid-state NMR reveals structural differences between fibrils of wild-type and disease-related A53T mutant α-synuclein. *J. Mol. Biol.* **380,** 444–450
35. Del Mar, C., Greenbaum, E. A., Mayne, L., Englander, S. W., and Woods, V. L., Jr. (2005) Structure and properties of α-synuclein and other amyloids determined at the amino acid level. *Proc. Natl. Acad. Sci. U.S.A.* **102,** 15477–15482

36. Der-Sarkissian, A., Jao, C. C., Chen, J., and Langen, R. (2003) Structural organization of α-synuclein fibrils studied by site-directed spin labeling. *J. Biol. Chem.* **278,** 37530–37535
37. Chen, M., Margittai, M., Chen, J., and Langen, R. (2007) Investigation of α-synuclein fibril structure by site-directed spin labeling. *J. Biol. Chem.* **282,** 24970–24979
38. Miake, H., Mizusawa, H., Iwatsubo, T., and Hasegawa, M. (2002) Biochemical characterization of the core structure of α-synuclein filaments. *J. Biol. Chem.* **277,** 19213–19219
39. Rodriguez, J. A., Ivanova, M. I., Sawaya, M. R., Cascio, D., Reyes, F. E., Shi, D., Sangwan, S., Guenther, E. L., Johnson, L. M., Zhang, M., Jiang, L., Arbing, M. A., Nannenga, B. L., Hattne, J., Whitelegge, J., *et al*. (2015) Structure of the toxic core of α-synuclein from invisible crystals. *Nature* **525,** 486–490
40. Wood, S. J., Wypych, J., Steavenson, S., Louis, J. C., Citron, M., and Biere, A. L. (1999) α-Synuclein fibrillogenesis is nucleation-dependent: Implications for the pathogenesis of Parkinson's disease. *J. Biol. Chem.* **274,** 19509–19512
41. Tycko, R. (2014) Physical and structural basis for polymorphism in amyloid fibrils. *Protein Sci.* **23,** 1528–1539
42. Qiang, W., Kelley, K., and Tycko, R. (2013) Polymorph-specific kinetics and thermodynamics of β-amyloid fibril growth. *J. Am. Chem. Soc.* **135,** 6860–6871
43. Bieschke, J., Herbst, M., Wiglenda, T., Friedrich, R. P., Boeddrich, A., Schiele, F., Kleckers, D., Lopez del Amo, J. M., Grüning, B. A., Wang, Q., Schmidt, M. R., Lurz, R., Anwyl, R., Schnoegl, S., Fändrich, M., *et al*. (2011) Small-molecule conversion of toxic oligomers to nontoxic β-sheet-rich amyloid fibrils. *Nat. Chem. Biol.* **8,** 93–101
44. Jameson, L. P., Smith, N. W., and Dzyuba, S. V. (2012) Dye-binding assays for evaluation of the effects of small molecule inhibitors on amyloid (aβ) self-assembly. *ACS Chem. Neurosci.* **3,** 807–819
45. Jiang, L., Liu, C., Leibly, D., Landau, M., Zhao, M., Hughes, M. P., and Eisenberg, D. S. (2013) Structure-based discovery of fiber-binding compounds that reduce the cytotoxicity of amyloid β. *Elife.* **2,** e00857
46. Ehrnhoefer, D. E., Bieschke, J., Boeddrich, A., Herbst, M., Masino, L., Lurz, R., Engemann, S., Pastore, A., and Wanker, E. E. (2008) EGCG redirects amyloidogenic polypeptides into unstructured, off-pathway oligomers. *Nat. Struct. Mol. Biol.* **15,** 558–566
47. Bieschke, J., Russ, J., Friedrich, R. P., Ehrnhoefer, D. E., Wobst, H., Neugebauer, K., and Wanker, E. E. (2010) EGCG remodels mature α-synuclein and amyloid-β fibrils and reduces cellular toxicity. *Proc. Natl. Acad. Sci. U.S.A.* **107,** 7710–7715
48. Lam, H. T., Graber, M. C., Gentry, K. A., and Bieschke, J. (2016) Stabilization of α-synuclein fibril clusters prevents fragmentation and reduces seeding activity and toxicity. *Biochemistry* **55,** 675–685
49. Cohen, S. I. A., Arosio, P., Presto, J., Kurudenkandy, F. R., Biverstal, H., Dolfe, L., Dunning, C., Yang, X., Frohm, B., Vendruscolo, M., Johansson, J., Dobson, C. M., Fisahn, A., Knowles, T. P. J., and Linse, S. (2015) A molecular chaperone breaks the catalytic cycle that generates toxic Aβ oligomers. *Nat. Struct. Mol. Biol.* **22,** 207–213
50. LeVine, H., 3rd (1993) Thioflavine T interaction with synthetic Alzheimer's disease β-amyloid peptides: Detection of amyloid aggregation in solution. *Protein Sci.* **2,** 404–410
51. Biancalana, M., Makabe, K., Koide, A., and Koide, S. (2009) Molecular mechanism of thioflavin-T binding to the surface of beta-rich peptide self-assemblies. *J. Mol. Biol.* **385,** 1052–1063
52. D'Amico, M., Di Carlo, M. G., Groenning, M., Militello, V., Vetri, V., and Leone, M. (2012) Thioflavin T promotes Aβ(1–40) amyloid fibrils formation. *J. Phys. Chem. Lett.* **3,** 1596–1601
53. Coelho-Cerqueira, E., Pinheiro, A. S., and Follmer, C. (2014) Pitfalls associated with the use of Thioflavin-T to monitor anti-fibrillogenic activity. *Bioorg. Med. Chem. Lett.* **24,** 3194–3198
54. Chirgadze, Y. N., and Nevskaya, N. A. (1976) Infrared spectra and resonance interaction of amide-I vibration of the antiparallel-chain pleated sheet. *Biopolymers* **15,** 607–625
55. Zandomeneghi, G., Krebs, M. R., McCammon, M. G., and Fändrich, M. (2004) FTIR reveals structural differences between native β-sheet proteins and amyloid fibrils. *Protein Sci.* **13,** 3314–3321
56. Winner, B., Jappelli, R., Maji, S. K., Desplats, P. A., Boyer, L., Aigner, S., Hetzer, C., Loher, T., Vilar, M., Campioni, S., Tzitzilonis, C., Soragni, A., Jessberger, S., Mira, H., Consiglio, A., *et al*. (2011) *In vivo* demonstration that α-synuclein oligomers are toxic. *Proc. Natl. Acad. Sci. U.S.A.* **108,** 4194–4199
57. Cremades, N., Cohen, S. I., Deas, E., Abramov, A. Y., Chen, A. Y., Orte, A., Sandal, M., Clarke, R. W., Dunne, P., Aprile, F. A., Bertoncini, C. W., Wood, N. W., Knowles, T. P., Dobson, C. M., and Klenerman, D. (2012) Direct observation of the interconversion of normal and toxic forms of α-synuclein. *Cell* **149,** 1048–1059
58. Danzer, K. M., Haasen, D., Karow, A. R., Moussaud, S., Habeck, M., Giese, A., Kretzschmar, H., Hengerer, B., and Kostka, M. (2007) Different species of α-synuclein oligomers induce calcium influx and seeding. *J. Neurosci.* **27,** 9220–9232
59. Conway, K. A., Lee, S. J., Rochet, J. C., Ding, T. T., Harper, J. D., Williamson, R. E., and Lansbury, P. T., Jr. (2000) Accelerated oligomerization by Parkinson's disease linked α-synuclein mutants. *Ann. N.Y. Acad. Sci.* **920,** 42–45
60. Conway, K. A., Lee, S. J., Rochet, J. C., Ding, T. T., Williamson, R. E., and Lansbury, P. T., Jr. (2000) Acceleration of oligomerization, not fibrillization, is a shared property of both α-synuclein mutations linked to early-onset Parkinson's disease: Implications for pathogenesis and therapy. *Proc. Natl. Acad. Sci. U.S.A.* **97,** 571–576
61. Pieri, L., Madiona, K., Bousset, L., and Melki, R. (2012) Fibrillar α-synuclein and huntingtin exon 1 assemblies are toxic to the cells. *Biophys. J.* **102,** 2894–2905
62. Peelaerts, W., Bousset, L., Van der Perren, A., Moskalyuk, A., Pulizzi, R., Giugliano, M., Van den Haute, C., Melki, R., and Baekelandt, V. (2015) α-Synuclein strains cause distinct synucleinopathies after local and systemic administration. *Nature* **522,** 340–344
63. Kumar, S., Mohanty, S. K., and Udgaonkar, J. B. (2007) Mechanism of formation of amyloid protofibrils of barstar from soluble oligomers: Evidence for multiple steps and lateral association coupled to conformational conversion. *J. Mol. Biol.* **367,** 1186–1204
64. Sekhar, A., and Udgaonkar, J. B. (2011) Fluoroalcohol-induced modulation of the pathway of amyloid protofibril formation by barstar. *Biochemistry* **50,** 805–819
65. Frimpong, A. K., Abzalimov, R. R., Uversky, V. N., and Kaltashov, I. A. (2010) Characterization of intrinsically disordered proteins with electrospray ionization mass spectrometry: Conformational heterogeneity of α-synuclein. *Proteins* **78,** 714–722
66. Sandal, M., Valle, F., Tessari, I., Mammi, S., Bergantino, E., Musiani, F., Brucale, M., Bubacco, L., and Samorì, B. (2008) Conformational equilibria in monomeric α-synuclein at the single-molecule level. *PLoS Biol.* **6,** e6
67. Gurry, T., Ullman, O., Fisher, C. K., Perovic, I., Pochapsky, T., and Stultz, C. M. (2013) The dynamic structure of α-synuclein multimers. *J. Am. Chem. Soc.* **135,** 3865–3872
68. Kumar, S., and Udgaonkar, J. B. (2009) Structurally distinct amyloid protofibrils form on separate pathways of aggregation of a small protein. *Biochemistry* **48,** 6441–6449
69. Zhang, Z., and Smith, D. L. (1993) Determination of amide hydrogen exchange by mass spectrometry: A new tool for protein structure elucidation. *Protein Sci.* **2,** 522–531
70. Jain, S., and Udgaonkar, J. B. (2010) Salt-induced modulation of the pathway of amyloid fibril formation by the mouse prion protein. *Biochemistry* **49,** 7615–7624
71. Krebs, M. R., Bromley, E. H., and Donald, A. M. (2005) The binding of thioflavin-T to amyloid fibrils: Localisation and implications. *J. Struct. Biol.* **149,** 30–37
72. Wu, C., Biancalana, M., Koide, S., and Shea, J. E. (2009) Binding modes of thioflavin-T to the single-layer β-sheet of the peptide self-assembly mimics. *J. Mol. Biol.* **394,** 627–633
73. Ivancic, V. A., Ekanayake, O., and Lazo, N. D. (2016) Binding modes of thioflavin T on the surface of amyloid fibrils studied by NMR. *Chemphyschem* **17,** 2461–2464
74. Mao, X., Guo, Y., Wang, C., Zhang, M., Ma, X., Liu, L., Niu, L., Zeng, Q., Yang, Y., and Wang, C. (2011) Binding modes of thioflavin T molecules to

prion peptide assemblies identified by using scanning tunneling microscopy. *ACS Chem. Neurosci.* **2,** 281–287

75. Rodríguez-Rodríguez, C., Rimola, A., Rodríguez-Santiago, L., Ugliengo, P., Alvarez-Larena, A., Gutiérrez-de-Terán, H., Sodupe, M., and González-Duarte, P. (2010) Crystal structure of thioflavin-T and its binding to amyloid fibrils: Insights at the molecular level. *Chem. Commun.* (*Camb.*) **46,** 1156–1158
76. Li, S., Liu, F. F., Yu, L. L., Zhao, Y. J., and Dong, X. Y. (2016) Dual effect of thioflavin T on the nucleation kinetics of amyloid β-protein 40. *Acta Phys. Chim. Sin.* **32,** 1391–1396
77. Hoyer, W., Cherny, D., Subramaniam, V., and Jovin, T. M. (2004) Impact of the acidic C-terminal region comprising amino acids 109–140 on α-synuclein aggregation *in vitro*. *Biochemistry* **43,** 16233–16242
78. van Rooijen, B. D., van Leijenhorst-Groener, K. A., Claessens, M. M., and Subramaniam, V. (2009) Tryptophan fluorescence reveals structural features of α-synuclein oligomers. *J. Mol. Biol.* **394,** 826–833
79. Mysling, S., Betzer, C., Jensen, P. H., and Jorgensen, T. J. (2013) Characterizing the dynamics of α-synuclein oligomers using hydrogen/deuterium exchange monitored by mass spectrometry. *Biochemistry* **52,** 9097–9103
80. Okazaki, H., Ohori, Y., Komoto, M., Lee, Y. H., Goto, Y., Tochio, N., and Nishimura, C. (2013) Remaining structures at the N- and C-terminal regions of α-synuclein accurately elucidated by amide-proton exchange NMR with fitting. *FEBS Lett.* **587,** 3709–3714
81. Wu, K. P., and Baum, J. (2010) Detection of transient interchain interactions in the intrinsically disordered protein α-synuclein by NMR paramagnetic relaxation enhancement. *J. Am. Chem. Soc.* **132,** 5546–5547
82. Losasso, V., Pietropaolo, A., Zannoni, C., Gustincich, S., and Carloni, P. (2011) Structural role of compensatory amino acid replacements in the α-synuclein protein. *Biochemistry* **50,** 6994–7001
83. Dedmon, M. M., Lindorff-Larsen, K., Christodoulou, J., Vendruscolo, M., and Dobson, C. M. (2005) Mapping long-range interactions in α-synuclein using spin-label NMR and ensemble molecular dynamics simulations. *J. Am. Chem. Soc.* **127,** 476–477
84. Burré, J., Sharma, M., and Südhof, T. C. (2012) Systematic mutagenesis of α-synuclein reveals distinct sequence requirements for physiological and pathological activities. *J. Neurosci.* **32,** 15227–15242
85. Meuvis, J., Gerard, M., Desender, L., Baekelandt, V., and Engelborghs, Y. (2010) The conformation and the aggregation kinetics of α-synuclein depend on the proline residues in its C-terminal region. *Biochemistry* **49,** 9345–9352
86. Fernández, C. O., Hoyer, W., Zweckstetter, M., Jares-Erijman, E. A., Subramaniam, V., Griesinger, C., and Jovin, T. M. (2004) NMR of α-synuclein-polyamine complexes elucidates the mechanism and kinetics of induced aggregation. *EMBO J.* **23,** 2039–2046
87. Bertoncini, C. W., Jung, Y. S., Fernandez, C. O., Hoyer, W., Griesinger, C., Jovin, T. M., and Zweckstetter, M. (2005) Release of long-range tertiary interactions potentiates aggregation of natively unstructured α-synuclein. *Proc. Natl. Acad. Sci. U.S.A.* **102,** 1430–1435
88. Uversky, V. N., Li, J., and Fink, A. L. (2001) Metal-triggered structural transformations, aggregation, and fibrillation of human α-synuclein: A possible molecular NK between Parkinson's disease and heavy metal exposure. *J. Biol. Chem.* **276,** 44284–44296
89. Sabaté, R., Lascu, I., and Saupe, S. J. (2008) On the binding of Thioflavin-T to HET-s amyloid fibrils assembled at pH 2. *J. Struct. Biol.* **162,** 387–396
90. Huang, C., Ren, G., Zhou, H., and Wang, C. (2005) A new method for purification of recombinant human α-synuclein in *Escherichia coli*. *Protein Expr. Purif.* **42,** 173–177
91. Singh, J., Sabareesan, A. T., Mathew, M. K., and Udgaonkar, J. B. (2012) Development of the structural core and of conformational heterogeneity during the conversion of oligomers of the mouse prion protein to worm-like amyloid fibrils. *J. Mol. Biol.* **423,** 217–231